

1 **Quantitative framework for preferential flow initiation**
2 **and partitioning**

3 **John R. Nimmo**

4 U.S. Geological Survey

5 345 Middlefield Rd., MS-420

6 Menlo Park, CA 94025 USA

7 Phone 1-650-329-4537

8 Email jrnimmo@usgs.gov

9

10 **Key words:** unsaturated zone, preferential flow, macropore, micropore, matrix, infiltration,
11 runoff

12 **Impact statement:** A quantitative framework based on spatially variable soil properties
13 facilitates the prediction of preferential flow in soils, a critical process affecting soil function and
14 contaminant transport.

15 **Abbreviations:** STVF, surface-tension viscous-flow; REA, representative elementary area;
16 EMA, elementary matrix area; PFF, preferential flow fraction.

17

18 **Quantitative framework for preferential flow initiation** 19 **and partitioning**

20 **Abstract**

21 A model for preferential flow in macropores is based on the short-range spatial distribution
22 of soil matrix infiltrability. It uses elementary areas at two different scales. One is the traditional
23 representative elementary area (REA), which includes a sufficient heterogeneity to typify larger
24 areas, as for measuring field-scale infiltrability. The other, called an elementary matrix area
25 (EMA), is smaller, but large enough to represent the local infiltrability of soil matrix material,
26 between macropores. When water is applied to the land surface, each EMA absorbs water up to
27 the rate of its matrix infiltrability. Excess water flows into a macropore, becoming preferential
28 flow. The land surface then can be represented by a mesoscale (EMA-scale) distribution of
29 matrix infiltrabilities. Total preferential flow at given depth is the sum of contributions from all
30 EMAs. Applying the model, one case study with multi-year field measurements of both
31 preferential and diffuse fluxes at a specific depth was used to obtain parameter values by inverse
32 calculation. The results quantify the preferential/diffuse partition of flow from individual storms
33 that differed in rainfall amount, intensity, antecedent soil water, and other factors. Another case
34 study provided measured values of matrix infiltrability to estimate parameter values for
35 comparison and illustrative predictions. These examples give a self-consistent picture from the
36 combination of parameter values, directions of sensitivities, and magnitudes of differences
37 caused by different variables. One major practical use of this model is to calculate the
38 dependence of preferential flow on climate-related factors such as varying soil wetness and
39 rainfall intensity.

40

41 **Impact statement:** A quantitative framework based on the spatial variability of infiltrability
42 of soil matrix material facilitates the prediction of the initiation and amount of preferential flow
43 in soils.

44 **Abbreviations:** STVF, surface-tension viscous-flow; REA, representative elementary area;
45 EMA, elementary matrix area; PFF, preferential flow fraction.

46 **Key words:** unsaturated zone, preferential flow, macropore, micropore, matrix, infiltration,
47 runoff

48 **Introduction**

49 When water is applied to the land surface, it is important to know whether and how much of
50 it goes into the subsurface as preferential flow. Fundamentally, preferential flow travels
51 significant distances along preferred paths that constitute a small fraction of the medium's
52 volume. Faster and less interactive with solid material than diffuse flow (Gerke, 2006; Jarvis,
53 2007), preferential flow is important to aquifer recharge rates, contaminant transport, soil-plant-
54 water relations, salt and nutrient distributions in the root zone, hydromechanical phenomena such
55 as landslides, and subsurface stormflow. Practical needs concerning preferential flow include a
56 means of predicting its initiation, and the quantitative partitioning of flowing water into diffuse
57 and preferential modes.

58 Major influences on preferential flow include relatively stable factors such as the medium
59 and its hydraulic properties, and time-varying hydraulic conditions such as the soil water content
60 and the source of applied water (Heppell et al., 2002). Different flow behaviors arise from water
61 sources that are uniform or concentrated in space, or intensities that are low or high (Beven and
62 Germann, 1982; Pruess, 1999). Criteria for recognizing and predicting preferential flow must
63 account for diverse nonequilibrium processes and a wide range of moisture states (Thomas and

64 Phillips, 1979; Hendrickx and Flury, 2001; Jarvis, 2007). Types of preferential flow include
65 macropore flow (Aubertin, 1971), funneled flow (Kung, 1990), and fingered or unstable flow
66 (Hendrickx and Flury, 2001). This study emphasizes macropore flow, which often can include
67 the greatest portion of preferential flow, and whose quantitative representation may also serve for
68 other flow modes.

69 For initiation of macropore flow by water applied at the land surface, this study uses the
70 criterion that water enters macropores when the input rate (as from precipitation, irrigation,
71 snowmelt, or other sources) exceeds the infiltrability of the surrounding matrix (Beven and
72 Germann, 1982). Various researchers have used this or similar criteria (e.g. Bronstert and Plate,
73 1997; Kätterer et al., 2001; Dusek et al., 2008). Certain other commonly-used criteria, like
74 saturation of matrix or complete filling of macropores, constitute a special case of this more
75 inclusive criterion, and so do not have to be considered separately. It is important not to assume
76 that matrix saturation is required. Accumulated evidence (e.g. Aubertin, 1971; Quisenberry and
77 Phillips, 1976; Scotter and Kanchanasut, 1981; Andreini and Steenhuis, 1990; Hardie et al.,
78 2013), reviewed by Nimmo (2012) and Villholth et al. (1998), shows that preferential flow is
79 commonplace in soils whose moisture states are substantially less than saturated. Preferential
80 flow may be greater in drier media. In cracking soils, for example, macropores are largest when
81 the soil is dry. Hydrophobicity, which also can cause flow to be preferential (Ritsema and
82 Dekker, 1996), tends to be greater in drier soil.

83 Observations also show that hydrologically significant preferential flow can occur in
84 macropores that are partially water-filled, i.e. that air as well as water occupies their internal
85 space. Pore aperture then has much less importance, and the preferential fluxes do not depend on
86 the saturated hydraulic conductivity (Radulovich et al., 1992). Experimental investigations

87 including those of Su et al. (1999; 2003), Dragila and Weisbrod (2003), and Cey and Rudolph
88 (2009) have observed this effect. Further evidence comes from the general trend of field-
89 measured speeds of preferential flow (Nimmo, 2007) toward values that are seldom fast enough
90 to be explainable as gravity-driven Poiseuille flow through capillary diameters of the size
91 normally reckoned as macropores. This limited speed of preferential flow is what leads to the
92 calculation of small (tens of μm or less) effective conduit diameters in studies such as those of
93 Kung et al. (2005) and Germann and Hensel (2006). Investigators including Tokunaga et al.
94 (2000), Tuller and Or (2001), Hincapié and Germann (2009), and Nimmo (2010) have developed
95 models based on pores that are partially filled with water.

96 Research on preferential flow has always recognized, at least implicitly or qualitatively, the
97 importance of the partitioning between macropore and matrix modes of flow. One way to
98 quantify this partitioning is with a preferential flow fraction (PFF), defined as the fraction of
99 input water that at a given time is undergoing preferential flow. Alternatives exist, though in this
100 work I emphasize the PFF for a specific depth at which preferential flow occurs. This
101 quantification has considerable utility in applications from hydrology, agriculture, waste-
102 disposal, ecohydrology, and other fields (e.g. Heppell et al., 2002; van Schaik et al., 2008;
103 Perkins et al., 2011).

104 One way to estimate PFF uses measured resident concentrations of a conservative tracer in
105 soil some time after its application at the land surface (Tyner et al., 2007; Perkins et al., 2011).
106 Subsurface drainage from agricultural fields may provide data for PFF flux (e.g. Villholth and
107 Jensen, 1998; Kohler et al., 2003). Hillslope-runoff investigations can also produce analogous
108 quantities (e.g. Bronstert and Plate, 1997; Bronstert, 1999; Stone et al., 2008).

109 Previous research on the initiation and partitioning of preferential flow notably includes the
110 model of Weiler and Naef (2003). Their equation 3 takes macropore inflow to be proportional to
111 the difference between an applied rate of input and a maximum absorption limit of soil matrix
112 material, as discussed above. Weiler and Naef emphasize microtopography, and the area of soil
113 that feeds macropores. The model of Weiler (2005) has similarities, though differing in that it
114 relies to some extent on conditions of pondedness and specific macropore properties. Though not
115 explicitly centered on macropore flow, infiltration investigations of Langhans et al. (2011; 2013)
116 explored increases of infiltrability with increasing rainfall intensity. They developed concepts
117 related to the role of small-scale heterogeneity, utilizing the relation between localized
118 heterogeneity and larger-scale infiltrability developed by Hawkins and Cundy (1987) for runoff
119 quantification.

120 Specific objectives of this paper are to identify criteria for the initiation of macropore flow at
121 the land surface, and to develop a means of estimating the preferential flow fraction, based on
122 spatially variable soil properties, conditions, and the applied flux density. Emphasis is on areally-
123 uniform rainfall, though the framework applies also to irrigation, ponding, or other input modes.
124 Tests with measured data evaluate this framework's ability to realistically connect soil and storm
125 characteristics with PFF, and the practicality of its implementation.

126 **Framework for partitioning of land-surface input**

127 **Definitions and description**

128 **Matrix and macropore**

129 The soil matrix, which occupies most of the soil's volume, has numerous pores of limited
130 extent, for convenience called micropores. In these pores, surface tension¹ can create an effective

¹ In similar contexts, the commonly used but less general term is *capillarity*, the expression of surface tension for water surrounded by the walls of a rigid conduit.

131 driving force, supplemental to gravity, expressed as the gradient of matric potential. Flow within
132 the matrix is assumed to occur under surface-tension viscous-flow (STVF) conditions, in which
133 both gravity and matric potential gradients are significant for driving flow (Miller and Miller,
134 1956; Yang et al., 1988).

135 In the range of moderate to high water contents, surface tension or capillary forces exert a
136 major effect on the fullness of individual pores, in addition to generating driving force. For
137 example, by Haines jumps, pores toggle abruptly between a state of little water with essentially
138 negligible conductance, and a state of near-fullness with relatively large conductance. This
139 toggling leads to the common generalization that only the full pores contribute significantly to
140 flow.

141 Large aperture is a typical reason for a pore to function as a macropore; natural features like
142 shrink/swell cracks, wormholes, and rootholes can constitute preferential flow paths (e.g. Beven
143 and Germann, 1982; Coppola et al., 2012), but the correspondence between such observable
144 features and hydraulically-effective preferential flow paths is not complete or exact. Some wide
145 pores are ineffective flow paths because of poor connectivity. Some small-aperture pores
146 effectively convey preferential flow because they have long-range extent and good connectivity
147 (Bouma, 1981). Evidence suggests that downward-streaming water in forms such as films and
148 rivulets of thickness that may be a few 10s of microns or less, can convey significant preferential
149 flow (Kung et al., 2005; Germann and Hensel, 2006; Kung et al., 2006; Nimmo, 2010). Because
150 such streams do not fill the entire pore cross section, aperture-based criteria do not apply.
151 Micropores, being composed of the spaces between individual grains, naturally do not extend (in
152 the flow direction) much more than a single grain diameter. Macropores, in order to transmit
153 preferential flow, necessarily have lengths many times greater than one grain diameter.

154 For a wide pore that is completely water-filled, capillarity is not a major driving force
155 because its influence goes inversely with aperture size. For a wide or narrow macropore that is
156 incompletely water-filled, capillarity is likewise not a major influence because the air-water
157 interfaces do not extend across the aperture. Thus preferential flow in macropores is driven
158 predominantly by gravity, with capillary forces (hence matric potential gradients) being
159 relatively insignificant for flow in the direction of the path. (Capillary forces may, however, be
160 significant in a perpendicular direction, as for absorption into the matrix.) A macropore, then,
161 functions under viscous-flow (VF) but not STVF conditions.

162 For these reasons I adopt here a functional definition. A macropore that conveys preferential
163 flow is one in which gravity is the dominant driving force and substantial flow can be conveyed
164 when the pore is incompletely water-filled. The aperture can be small, possibly less than 100 μm ,
165 though the continuous length must be many grain-diameters long. Though not directly inclusive
166 of fingered or unstable flow, which are conveyed by a collection of adjacent pores, this definition
167 would typically include a large portion of preferential flow that occurs in soils and rocks.

168 Flow path

169 Initiation of preferential flow may occur at the land surface, as emphasized here.
170 Alternatively, it could be at an injection well, a perched water body that supplies water to
171 unsaturated material below, or a subsurface feature where water seeps from matrix to macropore.
172 The model in this paper could be readily adapted for such alternatives. Water that travels
173 preferentially to a specified depth is typically a fraction of the preferential flow initiated at the
174 land surface, because of macropore termination, matrix absorption, or other reasons. Dye-tracer
175 experiments often show these effects (e.g. van Schaik, 2009), and they have been treated
176 quantitatively by Nimmo and Mitchell (2013) in terms of varying matrix water content at depths

177 where domain transfer occurs. A rigorous treatment of PFF needs specific consideration of the
178 depth of interest, the choice of which depends on the application at hand.

179 **Characterization of the land surface**

180 The land surface is conceived predominantly as exposed, heterogeneous matrix. In this
181 sense, matrix material also includes rock outcrops or other virtually nonconductive features. The
182 area of macropore openings at the land surface typically would be negligible.

183 For separate treatment of matrix and macropore infiltration, two levels of elementary areas
184 require consideration. One is the commonly recognized representative elementary area (REA) of
185 land surface. It must include a representative sample of macropores as well as of the
186 heterogeneous matrix material. Its size depends on land-surface attributes, at minimum being
187 large enough that a measurement of infiltrability, or infiltration capacity, over this area would not
188 differ significantly from a measurement over a somewhat larger area within the same plot. To
189 include a representative distribution of macropores might require it to be several square meters or
190 more. Infiltrability measurements often are done over a smaller area, thus requiring numerous
191 measurements combined with appropriate averaging techniques to estimate the infiltrability of an
192 REA and hence of the larger plot (e.g. Wilson and Luxmoore, 1988; Nimmo et al., 2009; Perkins
193 et al., 2011).

194 The other important elementary area is a localized representative area appropriate for
195 characterizing the matrix material, here called an elementary matrix area (EMA). It must be large
196 enough to include many micropores, so as to have measureable soil hydraulic properties, and
197 small enough to exclude macropores. It is not intended to represent an area larger than itself.
198 Thus in terms of unsaturated-zone hydrology, the EMA is a mesoscale concept. It can feed
199 localized runoff or infiltrating water to a macropore entry point. The EMA has similarities to
200 other concepts of a localized water-collecting area, such as the macropore drainage area (MDA)

201 of Weiler and Naef (2003). In a quantitative field-scale preferential flow model, it is a
 202 convenience to assume that EMAs are effectively infinitesimal. This allows development in
 203 terms of a continuous distribution of EMAs within the REA, and is employed here. Each EMA
 204 has a matrix infiltrability, symbolized b , the maximum flux density [LT^{-1}] of input that the EMA
 205 can completely absorb directly into the matrix material. Besides varying spatially within the
 206 REA, b varies temporally with local water content and possibly other factors.

207 A statistically significant number of measurements could quantify the spatial distribution of
 208 b . Such values could be inferred from measurements of the infiltrability of individual aggregates.
 209 An infiltrometer small enough to exclude the influence of macropores (Hallett et al., 2004;
 210 Lipiec et al., 2009) also could indicate b . One might also employ a larger tension infiltrometer
 211 with applied tension adjusted appropriately to exclude macropore flow (e.g. Wilson and
 212 Luxmoore, 1988; Jarvis et al., 2013). Indirect determinations also might be practical, such as the
 213 inference of localized infiltrability from microtopography (Langhans et al., 2013).

214 **Flow processes**

215 **Sub-REA and REA scales**

216 At an EMA, input water infiltrates into matrix up to the infiltrability of the EMA:

$$217 \quad (1) \quad \begin{aligned} i &= q, & q &\leq b \\ &= b, & q &> b \end{aligned}$$

218 where i is the infiltration flux density into the matrix material and q is the flux density of input
 219 water applied to the EMA. Excess water (w) left over from matrix infiltration then is

$$220 \quad (2) \quad \begin{aligned} w &= 0, & q &\leq b \\ &= q - b, & q &> b \end{aligned}$$

221 Entry into macropores is based on an assumption that this excess water has immediate access
 222 to a macropore entry point, as if adjacent to it. This assumption is not restricted to any particular

223 process that feeds the macropore. Localized overland flow is one plausible process. Another is
 224 that after infiltrating a short distance, perhaps a few mm or less, water may move laterally in
 225 shallow matrix material (Ritsema and Dekker, 1995). Such lateral flow might occur because the
 226 matrix immediately beneath it has extremely low K due to dryness, hydrophobicity, or other
 227 factors. It would be analogous to lateral movement of water immediately above the wetting front
 228 during conditions of saturation overshoot (Shiozawa and Fujimaki, 2004).

229 With this assumption that the excess from all EMAs is collectively available to macropores,
 230 the total effective excess for the REA is

$$231 \quad (3) \quad w_{eff} = \frac{1}{A} \iint_{REA} \max(q - b, 0) ds$$

232 where A is the area of the REA, s is a dummy variable of dimension L^2 , and the function
 233 $\max(x, y)$ designates the greater of x and y . In the absence of long-range runoff (beyond the
 234 REA), w_{eff} would flow into macropores. Figure 1 illustrates this matrix/macropore partitioning
 235 for hypothetical contrasting matrix materials.

236 The macropores within an REA have a collective infiltrability c , in terms of total volumetric
 237 flux per unit area of REA, which indicates the maximum rate of supplied water that the
 238 macropores can accept for preferential flow. In general c varies in time, for example with
 239 changes in shrink/swell cracks. Available water in excess of c becomes long-range runoff.
 240 Because excess input from EMAs flows into macropores of the REA up to the value of c ,

$$241 \quad (4) \quad \begin{aligned} j &= w_{eff}, & w_{eff} &\leq c \\ &= c, & w_{eff} &> c \end{aligned}$$

242 where j is the infiltration flux density into the macropores, collectively, of an REA. The excess
 243 over the combined capacities of the matrix and macropores of the REA becomes local ponding
 244 or runoff. Thus the runoff per unit area r from an REA is

$$(5) \quad \begin{aligned} r &= 0, & w_{eff} &\leq c \\ &= w_{eff} - c, & w_{eff} &> c \end{aligned}$$

246 REA and larger scales

247 Large-scale dynamics take into account such EMA characteristics as the spatial variability of
 248 localized infiltrability. The total infiltrability at the REA scale (symbolized l) equals the
 249 macropore infiltrability plus an effective matrix infiltrability b_{eff} :

$$(6) \quad l = c + b_{eff} = c + \frac{1}{A} \iint_{REA} b \, ds$$

251 At the REA scale, b_{eff} is the average of the EMA-scale b values.

252 Using continuum representations of both b and c over the land area, the bivariate distribution
 253 function $h(b,c)$ [T^2L^{-2}] can represent properties such that $h(\hat{b},\hat{c})dbdc$ is the relative abundance of
 254 area having

$$(7) \quad \begin{aligned} \hat{b} &\leq b < \hat{b} + db \\ \hat{c} &\leq c < \hat{c} + dc \end{aligned}$$

256 The function h is normalized such that

$$(8) \quad \iint_{00}^{\infty\infty} h(b,c) \, db \, dc = 1$$

258 This function is analogous to bivariate distribution functions used by Philip (1964) and Mualem
 259 (1974) for pore-scale properties. It could be represented by a cloud of probability density in 2-
 260 dimensional bc space.

261 To compute a property applicable over a particular area, $h(b,c)$ is integrated, weighted by the
 262 expression of that property, over the appropriate region of bc space. This procedure is closely
 263 analogous to that of Hawkins and Cundy (1987) for a univariate distribution of infiltration
 264 capacity. The effective matrix infiltration flux density over the REA is

$$(9) \quad i_{eff} = \iint_{00}^{\infty\infty} i h(b, c) db dc = \iint_{00}^{\infty q} b h(b, c) db dc + q \iint_{0q}^{\infty\infty} h(b, c) db dc$$

The collective macropore infiltration flux density over the REA is

$$(10) \quad j = \iint_{00}^{qq} c h(b, c) db dc + \iint_{q0}^{\infty q} (q - b) h(b, c) db dc$$

Runoff per unit area of REA is

$$(11) \quad r = \iint_{00}^{qq} (q - c) h(b, c) db dc$$

Thus, at a given time these formulas predict the partitioning of input q into matrix infiltration, preferential flow, and runoff. Note also that w_{eff} can be calculated as

$$(12) \quad w_{eff} = j + r = \iint_{00}^{qq} q h(b, c) db dc + \iint_{q0}^{\infty q} (q - b) h(b, c) db dc$$

These predictions require a known valuation of $h(b, c)$, i.e. the distribution of matrix infiltrability and macropore infiltrability, to characterize the land surface at a given time. Matrix infiltrability could likely be determined as noted above in the section on land-surface characterization. For macropore infiltrability c , the measurement is not as straightforward because it involves numerous macropores that are separated in space. Given a measurement of b_{eff} and l over a suitably large area, eq. (6) can be applied to give c by subtraction. A parameterized $h(b, c)$ could be calculated by inverse modeling from field measurements, though an extensive data set would be required, ideally with separate i_{eff} , j , and r values for a range of q .

For practicality of application and testing within the scope of this study, from here on this paper considers the limiting case of large c , such that there is no runoff. In this case the univariate distribution function

$$(13) \quad g(b) = \int_0^{\infty} h(b, c) dc$$

286 can represent the needed land-surface properties. This restricted model can separately predict the
 287 partitioning of infiltration into matrix and macropore components in the many situations where
 288 runoff is negligible. The matrix infiltration flux density is

$$289 \quad (14) \quad i_{eff} = \int_0^q b g(b) db + q \int_q^\infty g(b) db$$

290 and the macropore infiltration flux density is

$$291 \quad (15) \quad j = q - i_{eff} = \int_0^q (q - b) g(b) db$$

292 Figure 2 shows a graphical interpretation of formulas (14) and (15) applied at a given time,
 293 when rainfall intensity has the value q . The value of $g(b)$ is proportional to the abundance of area
 294 within the REA that has matrix infiltrability b . Where $b > q$, all input water goes to matrix flow,
 295 given by the second integral on the right side of (14) and labeled as Region I in the figure. For
 296 the range of $b < q$, at each value of b , a fraction b/q of the input flux density goes to matrix
 297 infiltration, and the remainder to macropores. This distinction divides this range into two regions
 298 of integration, separated by the curve $(b/q)g(b)$. Below this curve, region II represents matrix
 299 infiltration, the first integral on the right side of (14). Above this curve, region III represents
 300 macropore infiltration, the integral in (15).

301 The distribution function $g(b)$ can be parameterized for convenience. Examples in this paper
 302 employ a lognormal distribution, as commonly used for hydraulic conductivity distributions (e.g.
 303 Nielsen et al., 1973; Smith and Hebbert, 1979; Patin et al., 2012):

$$304 \quad (16) \quad g(b) = \frac{1}{b\sigma_g\sqrt{2\pi}} \exp\left[-\frac{(\ln(b)-\mu_g)^2}{2\sigma_g^2}\right]$$

305 Two parameters represent the distribution of b values: μ_g , the geometric mean of the distribution,
 306 and σ_g , its geometric standard deviation. The calculation of $g(b)$ from a hypothetical or fitted

307 distribution of b values thus can be calculated by computing the normalized lognormal
308 probability function at each b value, and dividing by b .

309 **Case-study testing and applicability**

310 **Purpose and requirements**

311 Without known values of the $g(b)$ function, a fully predictive test of PFF estimation is not
312 possible. The objective here instead is to show how the developed framework provides a basis
313 for relating the occurrence and quantity of preferential flow to soil hydraulic properties, soil-
314 water conditions, and rainstorm characteristics. The first case study, using measured data suitable
315 for evaluation of $g(b)$ by inverse modeling, infers the relative importance of critical variables that
316 influence preferential flow, in order to evaluate the consistency of the overall picture that
317 emerges and the reasonableness of optimized parameter values. The second uses field
318 measurements of spatially varying matrix infiltrability to show how the model predicts the
319 amount of preferential flow as a function of storm intensity.

320 Data required for inverse calculation of $g(b)$ include the water input rate $q(t)$ and preferential
321 flux density $j(t)$ through a subsurface plane, over a range of conditions. Such measurements
322 could come from experiments using field-drainage outflow (e.g. Kung et al., 2005; Rosenbom et
323 al., 2010) or water table fluctuation (Salve et al., 2012), though it is rare to find the full range of
324 data types needed. Eguchi and Hasegawa (2008) published an unusually complete data set,
325 measured with a water balance/Darcian flux technique, used here for inverse modeling of $g(b)$.
326 Instruments included a rain gauge for $q(t)$, TDR probes for soil water content, and tensiometers
327 for matric potential. Eguchi and Hasegawa recorded data from an agricultural field in Tsukuba,
328 Japan at 0.5-h intervals. They calculated matrix flow $i(t)$ at 1-m depth with Darcy's law, using
329 $\theta(t)$ measured at 1-m depth, $K(\theta)$ previously measured on core samples from that depth, and

330 matric potential gradient computed from tensiometer measurements at 0.90 and 1.10 m depth.
 331 They determined soil water storage $S(t)$ from TDR measurement of average θ within the 0-1 m
 332 depth interval. By water-balance considerations, preferential flow $j(t)$ at 1-m depth was
 333 computed as

$$334 \quad (17) \quad j(t) = q(t) - i(t) - \frac{dS}{dt}$$

335 In their seven years of data, Eguchi and Hasegawa found 26 rainstorms that generated significant
 336 preferential flow.

337 Data for forward calculation of $g(b)$ are available from the investigation of Wilson and
 338 Luxmoore (1988). At 37 locations in a forested watershed in eastern Tennessee, USA, they
 339 measured the near-surface hydraulic conductivity under conditions of slight suction, interpreted
 340 as matrix infiltrability. A lognormal fit to the relative abundance of data as a function of the
 341 infiltrability gives a usable $g(b)$ function. Although no measurements of preferential flow are
 342 available to compare with model predictions, the model outputs can be compared with those
 343 obtained with the Eguchi and Hasegawa data set to further evaluate the model's usefulness and
 344 ability to generate a self-consistent and plausible quantification of preferential flow behavior.

345 Procedure

346 Application of the model with the data of Eguchi and Hasegawa (2008) is done on a storm-
 347 by-storm basis, as opposed to an instantaneous or fixed time-interval basis. A single storm
 348 includes multiple 0.5-h timesteps that each may have a different amount of rain, and hence a
 349 different q . For analysis of a storm by the method diagrammed in Figure 2, this raises the
 350 question of what q best characterizes it. One alternative is the average intensity q_{avg} :

$$351 \quad (18) \quad q_{avg} = \frac{1}{n\delta t} \sum_{i=1}^n R_i$$

352 where the storm lasts for n timesteps of duration δt in which the amount of precipitation is R_i [L].
 353 This would give a relatively small value, with little relative influence of the timesteps of greatest
 354 precipitation, which possibly have the greatest real effect. Another alternative is to use the
 355 maximum intensity $R_m/\delta t$, where m indexes the timestep of greatest R_i . This would give a larger
 356 value, though it neglects any influence of the rest of the storm's precipitation. A compromise
 357 used here is an intensity-weighted average. The precipitation of each timestep is weighted by the
 358 ratio of its intensity $R_i/\delta t$ to the average intensity

$$359 \quad (19) \quad q_{wtd} = \frac{1}{n\delta t} \sum_{i=1}^n R_i \left(\frac{\frac{R_i}{\delta t}}{q_{avg}} \right) = \frac{\sum_{i=1}^n R_i^2}{\delta t \sum_{i=1}^n R_i}$$

360 This value falls between q_{avg} and $R_m/\delta t$, and retains some sensitivity to the overall storm
 361 magnitude and average intensity, while being especially sensitive to the timesteps of greatest
 362 intensity.

363 Optimization for the calibration of parameters μ_g and σ_g of the lognormal distribution (16) is
 364 based on the objective of matching the given storm's model-calculated PFF to Eguchi and
 365 Hasegawa's measured value. Of the two lognormal-distribution parameters, it is necessary to
 366 vary only one, since we are optimizing to a single scalar value. The one chosen here is μ_g , which
 367 lends itself easily to an intuitive physical interpretation through its relation to the average b
 368 value. This leaves geometric mean σ_g to be assigned a value. This parameter is interpretable as
 369 the factor that μ_g would be multiplied or divided by to be one standard deviation away from the
 370 geometric mean. It must be greater than 1, which would give an infinitely narrow distribution.
 371 Too large a value would smear distributions out too flat on the b axis. The illustrations here use a
 372 value of 3.0 as a compromise that produces visually reasonable distributions. This choice is
 373 further evaluated below in terms of sensitivities and comparison to other data.

374 Results

375 Test with known values of PFF

376 For testing, five storms were chosen from the Tsukuba data set of Eguchi and Hasegawa.

377 Designated by year-month-day of the start of the storm, these are:

- 378 • 2001-10-10, the example highlighted by Eguchi and Hasegawa (2008, Figure 4).
- 379 • 2002-5-7, a storm on soil of moderate antecedent water content, with relatively low
380 intensity, yet likely to generate substantial preferential flow.
- 381 • 1998-9-21, a storm on soil of moderate antecedent water content, comparable to that of
382 2002-5-7 but with higher weighted intensity.
- 383 • 1998-2-20 (not in the tabulation of Eguchi and Hasegawa), a storm on soil of relatively
384 low antecedent water content, with moderate intensity, likely to generate moderate
385 preferential flow if the water content is a not major factor, but little preferential flow if it
386 is.
- 387 • 1998-9-30, a storm on soil of high antecedent water content, and of moderate intensity
388 comparable to that of 1998-2-20.

389 Table 1 lists relevant parameters of these storms. Antecedent water content is taken as the
390 measurement of average water content in the 0-1 m depth interval at the time precipitation starts.
391 The total precipitation is the sum of rain gauge measurements R_i at half-hour intervals. Weighted
392 intensity is from formula (19). For four of these storms, PFF is the value tabulated by Eguchi and
393 Hasegawa (2008, Table 2). For the storm of 1998-02-20, which is not in that table on account of
394 negligible preferential flow, PFF is calculated assuming the preferential flow is a small number
395 between 0 and the detection limit of the method that Eguchi and Hasegawa used. Figures 3-5
396 show the distributions optimized by selecting the value of μ_g such that the model-computed
397 value of PFF equals the data-based value in column 5 of Table 1.

398 Figure 3, for the storm highlighted by Eguchi and Hasegawa, shows the peak of the
399 optimized $g(b)$ distribution at a value of b substantially less than the weighted intensity of the
400 storm, so as to generate a substantial amount of preferential flow according to equation (15).
401 Figure 4, for storms of nearly equal antecedent water content but different weighted intensities,
402 shows the storm of greater intensity generates more preferential flow. The different weighted
403 intensity is the strongest visual difference in the two graphs. It is clear how the appropriately-
404 weighted integrations of the distribution function $g(b)$ represent the different portions of the
405 distribution responsible for preferential flow for different storm intensities. Figure 5, for storms
406 of nearly equal weighted intensity but different antecedent water content, shows the storm falling
407 on the wetter soil generates more preferential flow. The $g(b)$ distributions are strikingly different
408 in the two graphs, indicating that $g(b)$ depends sensitively on transient conditions of the soil.
409 This result suggests that the matrix capacity dominates the antecedent moisture influence in this
410 case; the wet matrix has less remaining capacity to absorb water, so more goes into preferential
411 flow.

412 For the storm of 2001-10-10, sensitivity calculations (Figure 6) show that the PFF is much
413 more sensitive to μ_g than to σ_g . The sensitivity to σ_g does become substantial when its value is
414 close to 1, but this exception occurs because $\sigma_g=1$ is the unrealistic case of a totally uniform
415 distribution of b , at which PFF=0. Thus for a large range, including the value of 3 assumed in
416 previous calculations, PFF determinations are largely unaffected by the value used for σ_g .

417 The parameter values, directions of sensitivities, and magnitudes of differences caused by the
418 variables in these examples give a self-consistent picture that plausibly represents the infiltration
419 and preferential flow characteristics of the site, according to expectations based on known effects
420 of preferential flow. The framework's parameterization of the characteristic property

421 distributions appropriately represent the effects of antecedent soil water and rainfall intensity, as
422 seen especially in Figures 4 and 5.

423 Test with known values of matrix infiltrability

424 Wilson and Luxmoore (1988) used tension infiltrometers, adjusted for application of water at
425 a matric potential of -2 cm-water, to measure soil matrix infiltrability at 37 locations over an area
426 of 0.47 ha. In terms of cumulative probability, these measurements are plotted as the point
427 symbols in Figure 7. A lognormal distribution with $\mu_g = 62.4$ mm/h and $\sigma_g = 2.78$, shown in the
428 figure as the curve of matching color, fits the data well. For comparison, the figure also includes
429 cumulative lognormal distributions inferred from the Eguchi and Hasegawa measurements, for
430 two storms of contrasting antecedent conditions. Figure 8 compares the corresponding $g(b)$
431 functions using the format of Figures 2-5. Differences between the results of the two studies
432 derive mainly from the greater prevailing infiltrability of the Tennessee soil. Results from the
433 two storms of Eguchi and Hasegawa again illustrate the strong influence of antecedent moisture.
434 Results for the storm on drier conditions at the Japanese site, reflecting the greater infiltrability in
435 matrix material associated with greater capacity to absorb water, are closer to the Tennessee
436 measurements. It still appears that, beyond effects of moisture conditions, the Tennessee soil has
437 basic structural differences that give it generally greater infiltrability.

438 Based on calculations using equation (15) with these three distributions, Figure 9 shows the
439 model-predicted fraction of precipitation that becomes preferential flow. The results differ
440 widely, showing that the characteristic matrix infiltrability distributions are a strong indicator of
441 preferential flow behavior for a given site and conditions. When wet, the Japanese soil has the
442 capability for very large amounts of preferential flow even at relatively modest intensities, likely
443 having serious implications for recharging fluxes and solute transport. The Tennessee soil

444 requires extremely high, and likely rare, storm intensity to generate a large proportion of
445 preferential flow. Even in this matrix-conductive soil, however, there is an indication of
446 preferential flow down to an intensity that is less, by a factor of 4, than the geometric mean
447 matrix infiltrability. The predicted PFF is small at such low intensities, but could still have
448 important consequences for contaminant transport.

449 **Discussion**

450 **Characteristics and interpretation**

451 The model developed here represents soil properties governing macropore flow generation
452 and partitioning based on the distribution of matrix infiltrability over the land surface. Optimized
453 for data sets where both preferential and matrix flow have been measured, it computes the
454 preferential/diffuse flow response to a given input flux. It does this through a quantification of
455 the spatial variability of matrix infiltrability, leading to different proportions of preferential flow,
456 diffuse flow, and runoff, for different intensities of precipitation.

457 The limited but successful tests performed with this model support various physical
458 assumptions that underlie it. Chief among these is that in determining the timing and magnitude
459 of macropore flow, the properties of the matrix material adjacent to a macropore are more
460 important than those of the macropore itself. Values of the matrix infiltrability b relate to such
461 properties as sorptivity, hydraulic conductivity, and hydrophobicity, and in effect also
462 topography.

463 Postulating immediate macropore accessibility and continuum relations for heterogeneous
464 soil properties, this model has no explicit reliance on macropore spacing. With these assumptions
465 the model sidesteps any need to determine inter-macropore distances or number-density of
466 macropores. Avoiding this need is advantageous because estimation of such properties would

467 require knowledge of *all* macropores within an area, which is difficult in practice, and also in
468 principle, given the lack of a universally accepted definition of macropore. The functional
469 definition used here relies on hydraulic measurements rather than assessment by visual
470 inspection or related means. While we do not yet know what range of pore aperture sizes this
471 might include, available evidence, as noted in the introduction, suggests a broader inclusion than
472 what is commonly employed.

473 The strong dependence of $g(b)$ on transient conditions of the soil is a useful insight into
474 preferential flow behavior of the cases explored here. It confirms the results of other
475 investigations that show antecedent soil moisture to influence preferential flow, and provides a
476 way to represent such dependences quantitatively. However, it complicates the problem of
477 characterizing the matrix infiltrability distribution, because one cannot assume a single
478 determination of $g(b)$ would serve for a given field site. With additional research, it may be
479 possible to parameterize a dependence on antecedent conditions. For example, μ_g might be
480 found to vary systematically with soil water content. The distribution could then be scaled for
481 this influence, giving it greater generality for the representation of a given site.

482 **Utility**

483 Results from this model clearly could be useful in combination with one of the many dual-
484 domain models of subsurface flow (Šimůnek et al., 2003). The predicted matrix and macropore
485 fluxes could directly specify inputs to diffuse and preferential domains. Given a finite valuation
486 of c , the model could also compute runoff. It could be connected to existing runoff models,
487 applying formulas (9)-(11) to compute the contribution to runoff from water inputs that vary in
488 magnitude and intensity.

489 Several choices made in this model's development facilitate its implementation. The model's
490 continuum treatment of interacting processes avoids the need to specify the size of contributing
491 area (here the EMA). The distribution functions $g(b)$ and $h(c)$ in effect represent the effects not
492 only of matrix hydraulic conductivity but also the topography and the capacity and effective
493 areal density of macropores. Greater topographic slope would cause smaller b . Greater spacing
494 of macropores would cause smaller c or greater b . Lumping these acknowledged influences
495 together means there are few parameters, appropriate for the sparseness of data typically
496 available to implement a preferential flow model.

497 Depth-dependent factors such as flowpath continuity, matrix water dynamics, and
498 macropore/matrix interaction influence preferential flow, as observed, for example, by Kulli et
499 al. (2003). Consequently, values of parameters such as μ_g and σ_g could vary with the choice of
500 the depth where the partition of fluxes is calculated. This depth can be selected for a particular
501 application. If the chosen depth is at the water table, the calculated preferential flow represents
502 recharge, if at the bottom of root zone, it represents the loss of water available to plants. Other
503 possibilities include an emplaced flow detector, for comparison with measurements; a perched
504 water body or other sensitive feature, for vulnerability assessment; a slippage plane, for
505 landslides or related phenomena; and a soil pipe network, for subsurface stormflow.

506 Further developments

507 One important extension of this research would be to adapt it for data in the form of a series
508 of equal-length timesteps, as opposed to treating each storm as an integral unit. The weighted
509 average of equation (19) includes some influence of the total amount, as well as the intensity, of
510 precipitation in the storm. It does not support an analysis of the individual effects of such factors,
511 however. Individual-timestep evaluation of the PFF would allow independent assessment of

512 these factors. It would additionally allow more detailed predictions, as for the variation of PFF
513 with rainfall intensity during a storm.

514 Simple extensions would be valuable for some cases. Macropore openings could constitute a
515 finite portion of an REA, appropriate where numerous large pores open at the land surface.
516 Spatial variability of water input could account for areally heterogeneous processes that occur
517 with nonuniform surface cover, rainfall, irrigation, or snowmelt.

518 For the distribution functions $g(b)$ and $h(b,c)$, one can use a different parametric form, for
519 example the exponential form used by Hawkins and Cundy (1987). Moreover, the general
520 framework is not limited to parameterized distributions; non-parametric functions would afford
521 greater generality. Superpositions are also likely to be useful. For example, when there is a
522 distinct categorization of surface types (perhaps leaf-litter/bare-soil/impermeable-rock), one
523 could use a different set of parameters for each type, and superimpose the set of resulting curves.
524 A particular use for this alternative would be to represent rock outcrops by adding a spike or
525 delta-function near $b = 0$ to the distribution function for the rock-free portion of soil surface.

526 Development of new capabilities requires more and better measured data concerning
527 preferential flow and the conditions that influence it (e.g. Dusek et al., 2008). Few existing data
528 sets quantify the partitioning into matrix and preferential flow as done by Eguchi and Hasegawa
529 (2008). Beyond that, what is especially needed are field studies that measure both the distribution
530 of matrix infiltrability and the quantity of preferential flow for a range of input and antecedent
531 conditions. Such data sets would permit a full predictive test of models like the one developed
532 here. Quantitative knowledge of the preferential proportion of flow is crucial; without it,
533 development of models to predict when and how much preferential flow occurs would be
534 impossible. Field experiments for this purpose need to be recognized as worth their cost, because

535 of the great importance of preferential flow to major problems of water supply and
536 contamination, and the inability of current science to predict it reliably.

537 **Conclusions**

538 This paper presents a process-level characterization of macropore-flow initiation based on
539 the principle that preferential flow can be predicted from the distribution of matrix infiltrability,
540 developed into a framework for quantifying the partition of unsaturated flow into diffuse and
541 preferential components. Hydraulic properties of soil matrix material, not the preferential flow
542 paths themselves, are the main controlling influence. Quantification of the heterogeneity of
543 matrix hydraulic properties is essential to the relationship between the amount of preferential
544 flow and the characteristics of rainfall, irrigation, or other water inputs. A central feature is the
545 representation of heterogeneous soil properties at a mesoscale that encompasses many
546 micropores but is smaller than the REA that would be appropriate for determination of traditional
547 infiltrability.

548 Few data sets have enough of the measurements needed for testing this framework. It has
549 been tested with inverse calculation of model parameters based on the extensive multicomponent
550 data set of Eguchi and Hasegawa (2008), showing that the framework quantifies the distribution
551 of infiltrabilities that control macropore flow. Infiltrability measurements by Wilson and
552 Luxmoore (1988) allow additional testing with forward calculation of parameters. The results
553 correspond well to the measured data and general expectations based on effects of preferential
554 flow, giving a self-consistent picture that plausibly represents infiltration and preferential flow.
555 The characteristic matrix infiltrability distributions are a strong indicator of preferential flow
556 behavior for a given site and conditions, and appropriately represent effects of antecedent soil
557 water and rainfall intensity.

558 This framework has immediate value for discerning the sensitivity of preferential flow to
 559 factors like soil wetness and precipitation intensity. Such studies, though difficult because of the
 560 diversity of factors that influence preferential flow, are a critical need in soil science and
 561 hydrology, intensified by the imperative to predict consequences of a changing climate.
 562 Ultimately, and especially as better field measurements become available, the framework
 563 presented in this paper would be valuable for predicting the occurrence and quantity of
 564 preferential flow.

565 **Acknowledgments**

566 I am grateful to Sadao Eguchi for providing detailed data in tabular form. Natalie Leibovitz
 567 and Zhengzheng Qin carried out many of the calculations needed for development and testing of
 568 the model presented here. The Hydrologic Research and Development Program and the National
 569 Research Program of the U.S. Geological Survey provided support for this research.

570 **Table**

571 **Table 1. Parameter values for five storms.**

572

Start date of storm	Antecedent θ	Total precipitation (mm)	Weighted $d q$ (mm/h)	PFF	μ_g (mm/h)	σ_g (mm/h)
2001-10-01	0.575	119.8	8.86	0.407	5.08	3.00
2002-05-07	0.598	59.4	5.22	0.210	6.24	3.00
1998-09-21	0.599	53.4	14.95	0.376	9.47	3.00
1998-02-20	0.587	40.1	4.75	0.017	28.15	3.00
1998-09-30	0.622	37.6	4.57	0.652	1.10	3.00

573

574

575 **References**

- 576 Andreini, M.S., and T.S. Steenhuis. 1990. Preferential paths of flow under conventional and
577 conservation tillage. *Geoderma* 46:85-102.
- 578 Aubertin, G.M. 1971. Nature and Extent of Macropores in Forest Soils and their Influence on
579 Subsurface Water Movement. Research Paper NE-192. USDA Forest Service. Upper
580 Darby, PA.
- 581 Beven, K., and P. Germann. 1982. Macropores and water flow in soils. *Water Resources*
582 *Research* 18:1311-1325.
- 583 Bouma, J. 1981. Comment on "Micro-, Meso-, and Macroporosity of Soil". *Soil Science Society*
584 *of America Journal* 45(6):1244-1245. 10.2136/sssaj1981.03615995004500060050x.
- 585 Bronstert, A., and E.J. Plate. 1997. Modelling of runoff generation and soil moisture dynamics
586 for hillslopes and micro-catchments. *Journal of Hydrology* 198(1-4):177-195.
- 587 Bronstert, A. 1999. Capabilities and limitations of detailed hillslope hydrological modelling.
588 *Hydrological Processes* 13(1):21-48.
- 589 Cey, E.E., and D.L. Rudolph. 2009. Field study of macropore flow processes using tension
590 infiltration of a dye tracer in partially saturated soils. *Hydrological Processes* 23:1768-
591 1779.
- 592 Coppola, A., H.H. Gerke, A. Comegna, A. Basile, and V. Comegna. 2012. Dual-permeability
593 model for flow in shrinking soil with dominant horizontal deformation. *Water Resources*
594 *Research* 48(8):W08527. 10.1029/2011wr011376.
- 595 Dragila, M.I., and N. Weisbrod. 2003. Parameters affecting maximum fluid transport in large
596 aperture fractures. *Advances in Water Resources* 26(12):1219-1228.
- 597 Dusek, J., H.H. Gerke, and T. Vogel. 2008. Surface Boundary Conditions in Two-Dimensional
598 Dual-Permeability Modeling of Tile Drain Bromide Leaching. *Vadose Zone Journal*
599 7(4):1287-1301. 10.2136/vzj2007.0175.
- 600 Eguchi, S., and S. Hasegawa. 2008. Determination and Characterization of Preferential Water
601 Flow in Unsaturated Subsoil of Andisol. *Soil Science Society of America Journal*
602 72(2):320-330.
- 603 Gerke, H.H. 2006. Preferential flow descriptions for structured soils. *Journal of Plant Nutrition*
604 *and Soil Science* 169(3):382-400.
- 605 Germann, P.F., and D. Hensel. 2006. Poiseuille Flow Geometry Inferred from Velocities of
606 Wetting Fronts in Soils. *Vadose Zone Journal* 5(3):867-876.
- 607 Hallett, P.D., N. Nunan, J.T. Douglas, and I.M. Young. 2004. Millimeter-Scale Spatial
608 Variability in Soil Water Sorptivity. *Soil Science Society of America Journal* 68(2):352-

- 609 358. 10.2136/sssaj2004.3520.
- 610 Hardie, M., S. Lisson, R. Doyle, and W. Cotching. 2013. Determining the frequency, depth and
611 velocity of preferential flow by high frequency soil moisture monitoring. *Journal of*
612 *Contaminant Hydrology* 144(1):66-77. <http://dx.doi.org/10.1016/j.jconhyd.2012.10.008>.
- 613 Hawkins, R.H., and T.W. Cundy. 1987. Steady-state analysis of infiltration and overland flow
614 for spatially varied hillslopes. *Journal of the American Water Resources Association*
615 23(2):251-256.
- 616 Hendrickx, J.M.H., and M. Flury. 2001. Uniform and preferential flow mechanisms in the vadose
617 zone. *In* National Research Council (ed.) *Conceptual Models of Flow and Transport in*
618 *the Fractured Vadose Zone*. National Academy Press, Washington, DC. p. 149-187.
- 619 Heppell, C.M., F. Worrall, T.P. Burt, and R.J. Williams. 2002. A classification of drainage and
620 macropore flow in an agricultural catchment. *Hydrological Processes* 16(1):27-46.
621 10.1002/hyp.282.
- 622 Hincapié, I.A., and P.F. Germann. 2009. Abstraction from infiltrating water content waves
623 during weak viscous flows. *Vadose Zone Journal* 8(4):891-901.
- 624 Jarvis, N., J. Koestel, I. Messing, J. Moeys, and A. Lindahl. 2013. Influence of soil, land use and
625 climatic factors on the hydraulic conductivity of soil. *Hydrology and Earth System*
626 *Sciences* 17(12):5185-5195. 10.5194/hess-17-5185-2013.
- 627 Jarvis, N.J. 2007. A review of non-equilibrium water flow and solute transport in soil
628 macropores: principles, controlling factors and consequences for water quality. *European*
629 *Journal of Soil Science* 58(3):523-546.
- 630 Kätterer, T., B. Schmied, K.C. Abbaspour, and R. Schulin. 2001. Single- and dual-porosity
631 modelling of multiple tracer transport through soil columns--effects of initial moisture
632 and mode of application. *European Journal of Soil Science* 52(1):25-36. 10.1046/j.1365-
633 2389.2001.00355.x.
- 634 Kohler, A., K.C. Abbaspour, M. Fritsch, and R. Schulin. 2003. Using Simple Bucket Models to
635 Analyze Solute Export to Subsurface Drains by Preferential Flow. *Vadose Zone Journal*
636 2(1):68-75. 10.2113/2.1.68.
- 637 Kulli, B., M. Gysi, and H. Flühler. 2003. Visualizing soil compaction based on flow pattern
638 analysis. *Soil and Tillage Research* 70(1):29-40. [http://dx.doi.org/10.1016/S0167-](http://dx.doi.org/10.1016/S0167-1987(02)00121-6)
639 [1987\(02\)00121-6](http://dx.doi.org/10.1016/S0167-1987(02)00121-6).
- 640 Kung, K.-J.S., M. Hanke, C.S. Helling, E.J. Kladvko, T.J. Gish, T.S. Steenhuis, and D.B.
641 Jaynes. 2005. Quantifying Pore-Size Spectrum of Macropore-Type Preferential
642 Pathways. *Soil Science Society of America Journal* 69(4):1196-1208.
- 643 Kung, K.-J.S., E.J. Kladvko, C.S. Helling, T.J. Gish, T.S. Steenhuis, and D.B. Jaynes. 2006.
644 Quantifying the Pore Size Spectrum of Macropore-Type Preferential Pathways under

- 645 Transient Flow. *Vadose Zone Journal* 5(3):978-989.
- 646 Kung, K.J.S. 1990. Preferential flow in a sandy vadose zone--1. Field observation. *Geoderma*
647 46(1/3):51-58. 1990-049956.
- 648 Langhans, C., G. Govers, J. Diels, A. Leys, W. Clymans, A.V.d. Putte, and J. Valckx. 2011.
649 Experimental rainfall-runoff data: Reconsidering the concept of infiltration capacity.
650 *Journal of Hydrology* 399(3-4):255-262. <http://dx.doi.org/10.1016/j.jhydrol.2011.01.005>.
- 651 Langhans, C., G. Govers, and J. Diels. 2013. Development and parameterization of an infiltration
652 model accounting for water depth and rainfall intensity. *Hydrological Processes*
653 27(25):3777-3790. 10.1002/hyp.9491.
- 654 Lipiec, J., A. Wójciga, and R. Horn. 2009. Hydraulic properties of soil aggregates as influenced
655 by compaction. *Soil and Tillage Research* 103(1):170-177.
656 <http://dx.doi.org/10.1016/j.still.2008.10.021>.
- 657 Miller, E.E., and R.D. Miller. 1956. Physical theory for capillary flow phenomena. *Journal of*
658 *Applied Physics* 27(4):324-332.
- 659 Mualem, Y. 1974. A conceptual model of hysteresis. *Water Resources Research* 10(3):514-520.
- 660 Nielsen, D.R., J.W. Biggar, and K.T. Erh. 1973. Spatial variability of field-measured soil-water
661 properties. *Hilgardia* 42(7):215-259.
- 662 Nimmo, J.R. 2007. Simple Predictions of Maximum Transport Rate in Unsaturated Soil and
663 Rock. *Water Resources Research* 43(5). 10.1029/2006wr005372.
- 664 Nimmo, J.R., K.S. Perkins, K.M. Schmidt, D.M. Miller, J.D. Stock, and K. Singha. 2009.
665 Hydrologic Characterization of Desert Soils with Varying Degrees of Pedogenesis -- I.
666 Field Experiments Evaluating Plant-Relevant Soil-Water Behavior. *Vadose Zone Journal*
667 8(2):480-495.
- 668 Nimmo, J.R. 2010. Theory for Source-Responsive and Free-Surface Film Modeling of
669 Unsaturated Flow. *Vadose Zone Journal* 9(2):295-306.
- 670 Nimmo, J.R. 2012. Preferential Flow Occurs in Unsaturated Conditions. *Hydrological Processes*
671 26(5):786-789.
- 672 Nimmo, J.R., and L. Mitchell. 2013. Predicting vertically nonsequential wetting patterns with a
673 source-responsive model. *Vadose Zone Journal* 12(4). 10.2136/vzj2013.03.0054.
- 674 Patin, J., E. Mouche, O. Ribolzi, V. Chaplot, O. Sengtahevong, K.O. Latsachak, B.
675 Souleuth, and C. Valentin. 2012. Analysis of runoff production at the plot scale during a
676 long-term survey of a small agricultural catchment in Lao PDR. *Journal of Hydrology*
677 426-427(0):79-92. <http://dx.doi.org/10.1016/j.jhydrol.2012.01.015>.
- 678 Perkins, K.S., J.R. Nimmo, C.E. Rose, and R.H. Coupe. 2011. Field tracer investigation of

- 679 unsaturated zone flow paths and mechanisms in agricultural soils of northwestern
680 Mississippi, USA. *Journal of Hydrology* 396(1-2):1-11.
- 681 Philip, J.R. 1964. Similarity hypothesis for capillary hysteresis in porous materials. *Journal of*
682 *Geophysical Research* 69(8):1553-1562. 10.1029/JZ069i008p01553.
- 683 Pruess, K. 1999. A mechanistic model for water seepage through thick unsaturated zones in
684 fractured rocks of low matrix permeability. *Water Resources Research* 35(4):1039-1051.
- 685 Quisenberry, V.L., and R.E. Phillips. 1976. Percolation of surface-applied water in the field. *Soil*
686 *Science Society of America Journal* 40(4):484-489.
- 687 Radulovich, R., P. Baveye, P. Sollins, and E. Solórzano. 1992. Bypass Water Flow through
688 Unsaturated Microaggregated Tropical Soils. *Soil Science Society of America Journal*
689 56(3):721-726. 10.2136/sssaj1992.03615995005600030008x.
- 690 Ritsema, C.J., and L.W. Dekker. 1995. Distribution Flow--A General Process in the Top Layer
691 of Water Repellent Soils. *Water Resources Research* 31(5):1187-1200.
692 10.1029/94wr02979.
- 693 Ritsema, C.J., and L.W. Dekker. 1996. Water repellency and its role in forming preferred flow
694 paths in soils. *Australian Journal of Soil Research* 34(4):475-487.
695 <http://dx.doi.org/10.1071/SR9960475>.
- 696 Rosenbom, A.E., W. Brüsch, R.K. Juhler, V. Ernstsén, L. Gudmundsson, J. Kjær, F. Plauborg, R.
697 Grant, P. Nyegaard, and P. Olsen. 2010. The Danish Pesticide Leaching Assessment
698 Programme Monitoring results May 1999–June 2009. Geological Survey of Denmark and
699 Greenland, Copenhagen.
- 700 Salve, R., D.M. Rempe, and W.E. Dietrich. 2012. Rain, rock moisture dynamics, and the rapid
701 response of perched groundwater in weathered, fractured argillite underlying a steep
702 hillslope. *Water Resources Research* 48(11). W11528. 10.1029/2012wr012583.
- 703 Scotter, D.R., and P. Kanchanasut. 1981. Anion movement in a soil under pasture. *Australian*
704 *Journal of Soil Research* 19(3):299-307. <http://dx.doi.org/10.1071/SR9810299>.
- 705 Shiozawa, S., and H. Fujimaki. 2004. Unexpected water content profiles under flux-limited one-
706 dimensional downward infiltration in initially dry granular media. *Water Resources*
707 *Research* 40(7). W07404. 10.1029/2003WR002197.
- 708 Šimůnek, J., N.J. Jarvis, M.T. van Genuchten, and A. Gärdenäs. 2003. Review and comparison
709 of models for describing non-equilibrium and preferential flow and transport in the
710 vadose zone. *Journal of Hydrology* 272(1):14-35.
- 711 Smith, R.E., and R.H.B. Hebbert. 1979. A Monte Carlo Analysis of the hydrologic effects of
712 spatial variability of infiltration. *Water Resources Research* 15(2):419-429.
713 10.1029/WR015i002p00419.

- 714 Stone, J.J., G.B. Paige, and R.H. Hawkins. 2008. Rainfall intensity-dependent infiltration rates
715 on rangeland rainfall simulator plots. *Transactions of the ASABE* 51(1):45-53.
- 716 Su, G.W., J.T. Geller, K. Pruess, and F. Wen. 1999. Experimental studies of water seepage and
717 intermittent flow in unsaturated, rough-walled fractures. *Water Resources Research*
718 35(4):1019-1037.
- 719 Su, G.W., J.R. Nimmo, and M.I. Dragila. 2003. Effect of isolated fractures on accelerated flow in
720 unsaturated porous rock. *Water Resources Research* 39(12). 10.1029/2002wr001691.
- 721 Thomas, G.W., and R.E. Phillips. 1979. Consequences of Water Movement in Macropores.
722 *Journal of Environmental Quality* 8(2):149-152.
- 723 Tokunaga, T.K., J. Wan, and S.R. Sutton. 2000. Transient film flow on rough fracture surfaces.
724 *Water Resources Research* 36(7):1737-1746.
- 725 Tuller, M., and D. Or. 2001. Hydraulic conductivity of variably saturated porous media--Film
726 and corner flow in angular pore space. *Water Resources Research* 37(5):1257-1276.
- 727 Tyner, J.S., W.C. Wright, and R.E. Yoder. 2007. Identifying Long-Term Preferential and Matrix
728 Flow Recharge at the Field Scale. *Transactions ASABE* 50(6):2001-2006.
- 729 van Schaik, N.L.M.B., S. Schnabel, and V.G. Jetten. 2008. The influence of preferential flow on
730 hillslope hydrology in a semi-arid watershed (in the Spanish Dehesas). *Hydrological*
731 *Processes* 22(18):3844-3855.
- 732 van Schaik, N.L.M.B. 2009. Spatial variability of infiltration patterns related to site
733 characteristics in a semi-arid watershed. *Catena* 78(1):36-47.
734 <http://dx.doi.org/10.1016/j.catena.2009.02.017>.
- 735 Villholth, K.G., K.H. Jensen, and J. Fredericia. 1998. Flow and transport processes in a
736 macroporous subsurface-drained glacial till soil--I. Field investigations. *Journal of*
737 *Hydrology* 207:98-120.
- 738 Villholth, K.G., and K.H. Jensen. 1998. Flow and transport processes in a macroporous
739 subsurface-drained glacial till soil--II. Model analysis. *Journal of Hydrology* 207:121-
740 135.
- 741 Weiler, M., and F. Naef. 2003. Simulating surface and subsurface initiation of macropore flow.
742 *Journal of Hydrology* 273(1-4):139-154. [http://dx.doi.org/10.1016/S0022-](http://dx.doi.org/10.1016/S0022-1694(02)00361-X)
743 [1694\(02\)00361-X](http://dx.doi.org/10.1016/S0022-1694(02)00361-X).
- 744 Weiler, M. 2005. An infiltration model based on flow variability in macropores: development,
745 sensitivity analysis and applications. *Journal of Hydrology* 310(1):294-315.
- 746 Wilson, G.V., and R.J. Luxmoore. 1988. Infiltration, macroporosity, and mesoporosity
747 distributions on two forested watersheds. *Soil Science Society of America Journal*
748 52(2):329-335.

749 Yang, Y.-W., G. Zograf, and E.E. Miller. 1988. Capillary flow phenomena and wettability in
750 porous media--II. Dynamic flow studies. *Journal of Colloid and Interface Science*
751 122(1):35-46. [http://dx.doi.org/10.1016/0021-9797\(88\)90285-8](http://dx.doi.org/10.1016/0021-9797(88)90285-8).

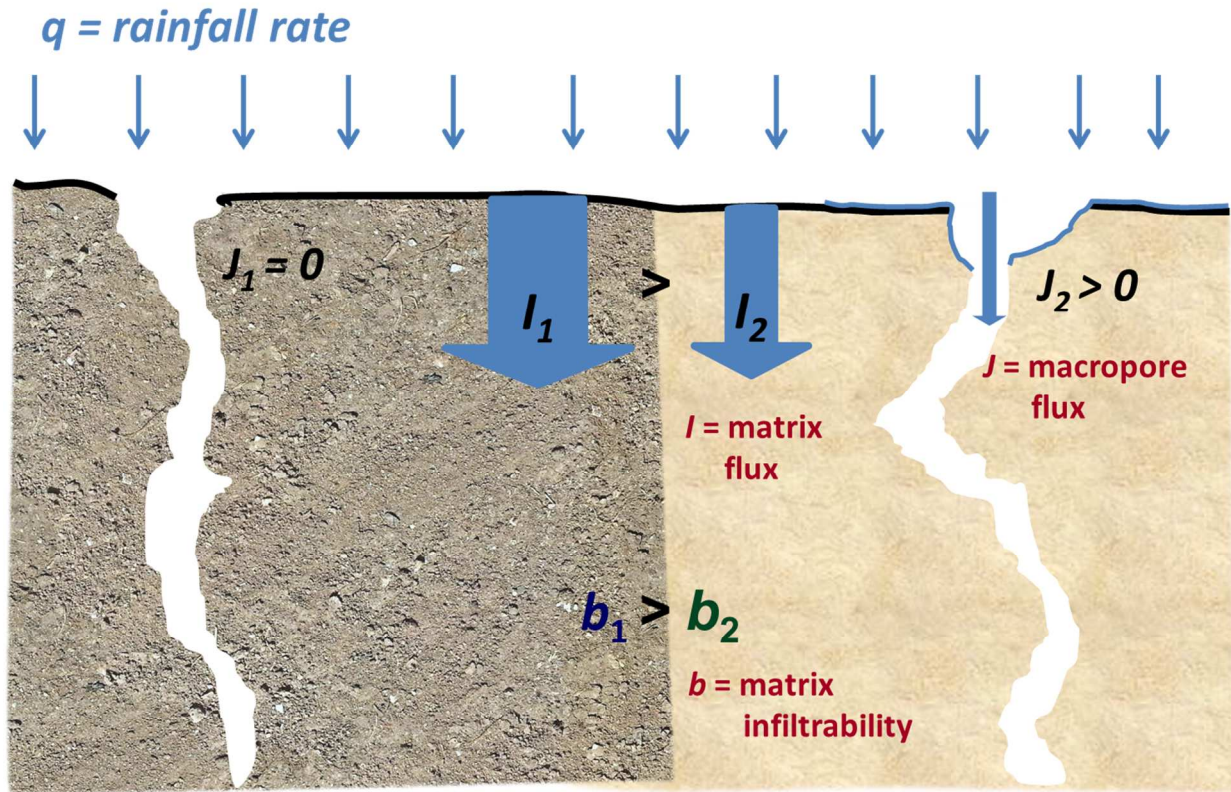
1
23
4
5
6
7

Figure 1. Macropore flow initiation, comparing adjacent parcels of soil that differ in matrix infiltrability.

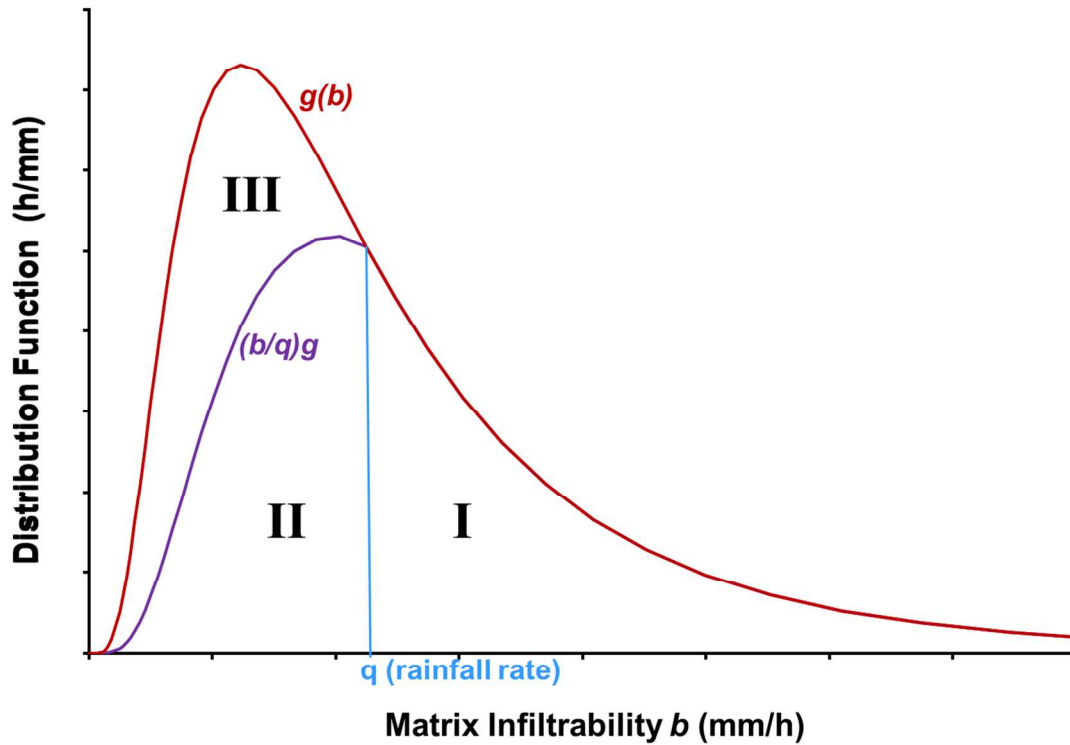


Figure 2. Hypothetical distribution of matrix infiltrability $g(b)$, within a representative elementary area of soil. Given rainfall at a rate q , the flow-partitioning framework in this paper divides the area under the $g(b)$ curve into three regions. A suitably-weighted integration of areas I and II predicts the effective matrix infiltration flux density as in equation (14), and of area III predicts the effective macropore infiltration flux density as in equation (15).

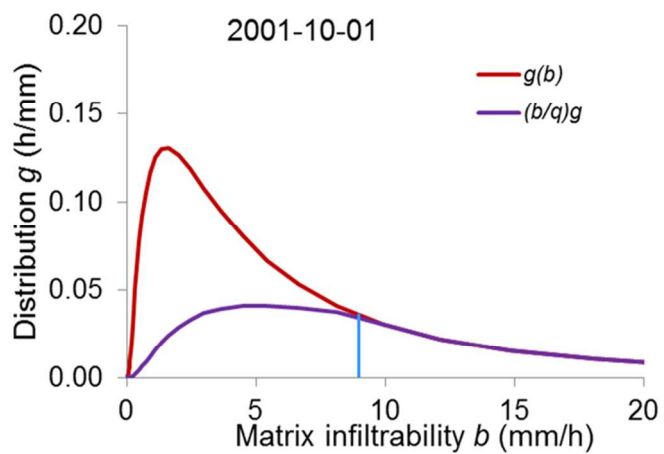


Figure 3. Distribution function $g(b)$ optimized to fit the matrix/preferential flow partitioning observed by Eguchi and Hasegawa (2008) for the storm beginning on 2001-10-1.

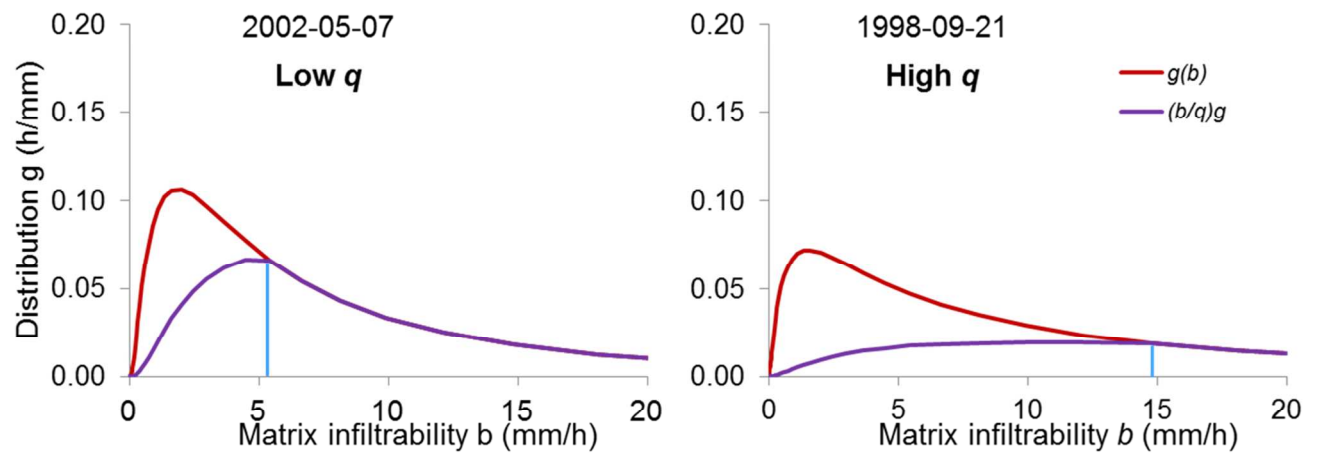


Figure 4. Distribution functions $g(b)$ optimized to fit the matrix/preferential flow partitioning observed by Eguchi and Hasegawa (2008) for the storms beginning on 2002-05-07 and 1998-09-21, both of which began when the 0-1 m average soil water content was 0.60. The weighted intensity of the two storms differed by nearly a factor of 3.

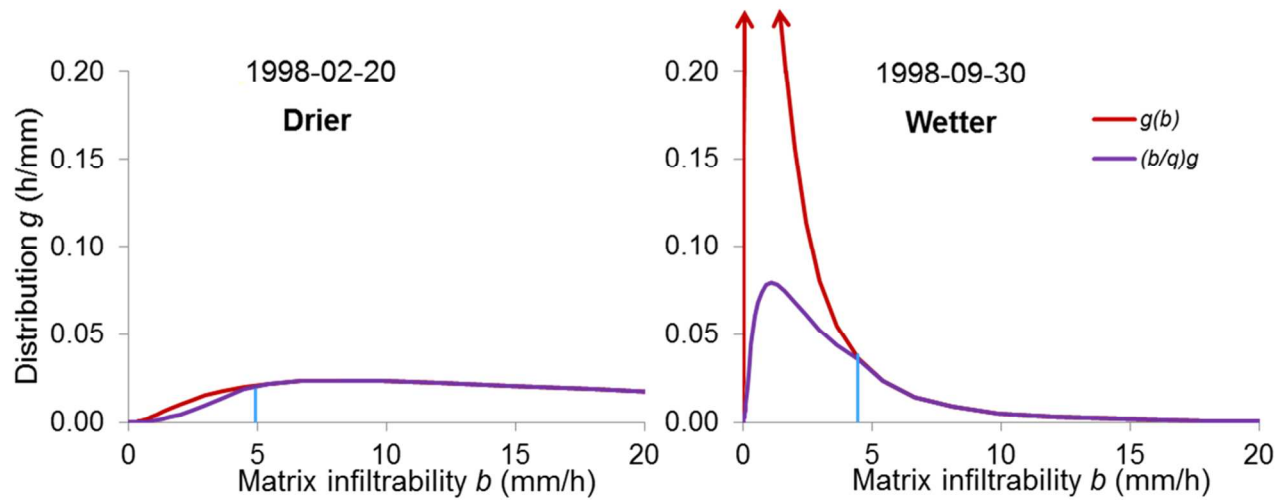
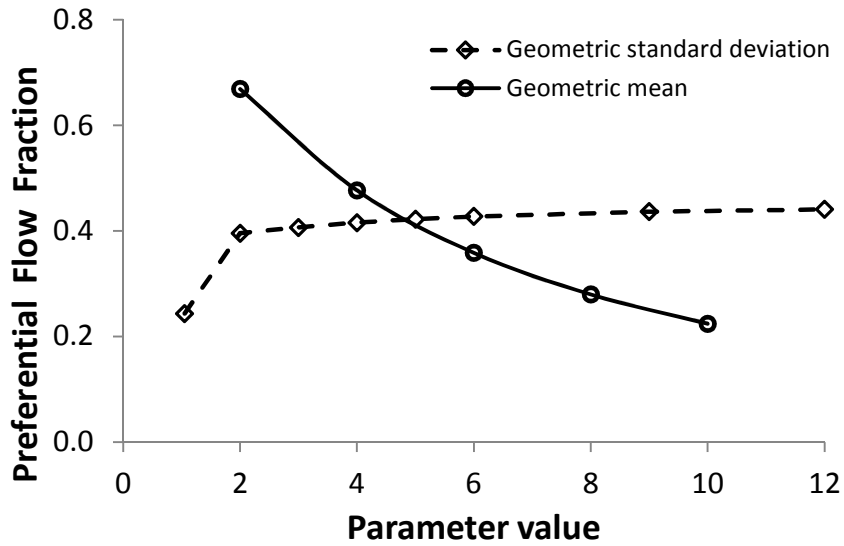


Figure 5. Distribution functions $g(b)$ optimized to fit the matrix/preferential flow partitioning observed by Eguchi and Hasegawa (2008) for the storms beginning on 1998-02-20 and 1998-09-30, which had nearly equal weighted intensity. The 1998-02-20 storm began with a significantly lower 0-1 m average soil water content.



1

2 **Figure 6. Sensitivity of PFF to parameter values of the lognormal distribution. For tests**
3 **with variation of the geometric mean, the geometric standard deviation was fixed at 3.0.**
4 **For tests with variation of the geometric standard deviation, the geometric mean was fixed**
5 **at 5.08 mm/h, the value optimized for the storm of 2001-10-01.**

6

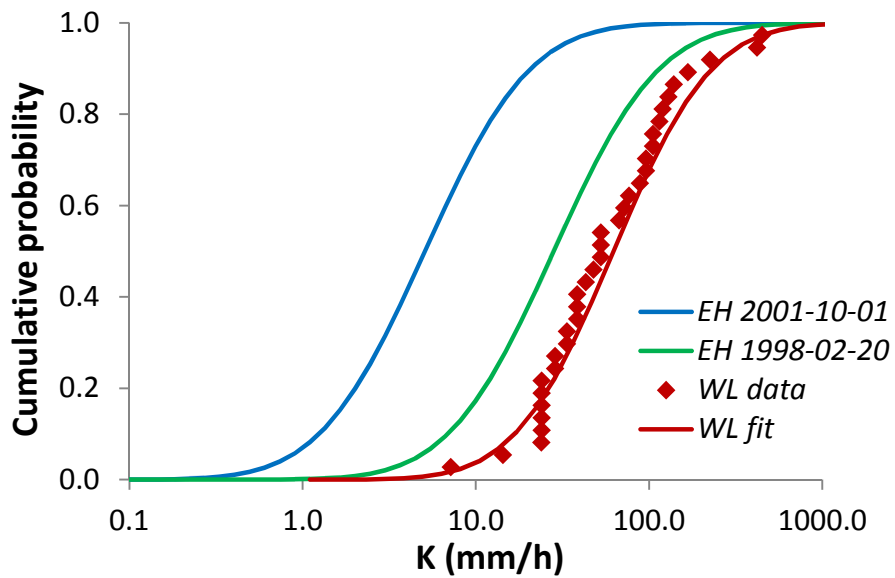


Figure 7. Cumulative lognormal probability distributions for measurements and lognormal fit to data of Wilson and Luxmoore (1988), and inferred probability distributions for effective matrix conductivities for two storms in the data of Eguchi and Hasegawa (2008) with wet (2001-10-01) and dry (1998-02-20) antecedent conditions.

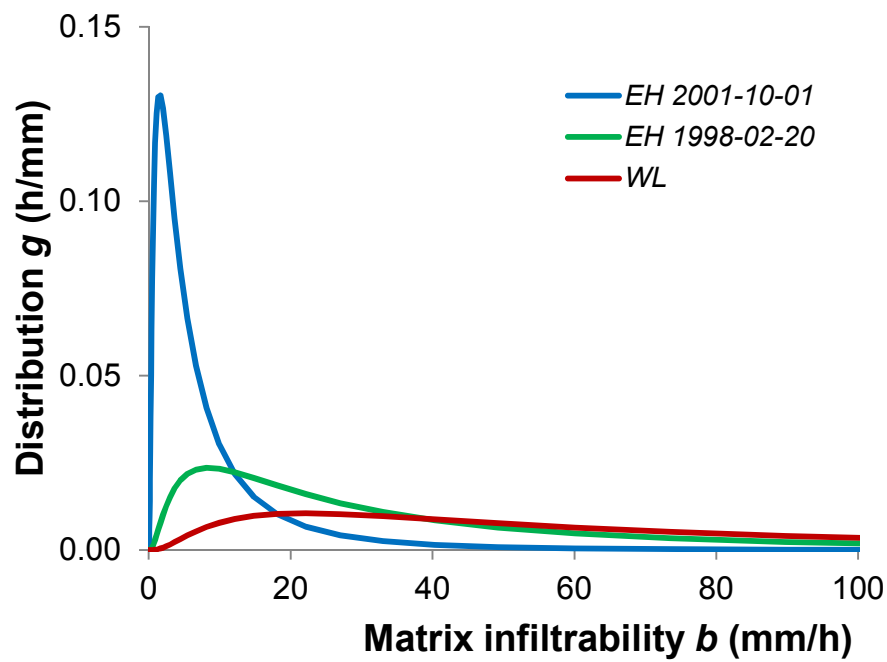


Figure 8. Computed lognormal distributions of matrix infiltrability fit to data of Wilson and Luxmoore (1988), and optimized for two storms in the data of Eguchi and Hasegawa (2008).

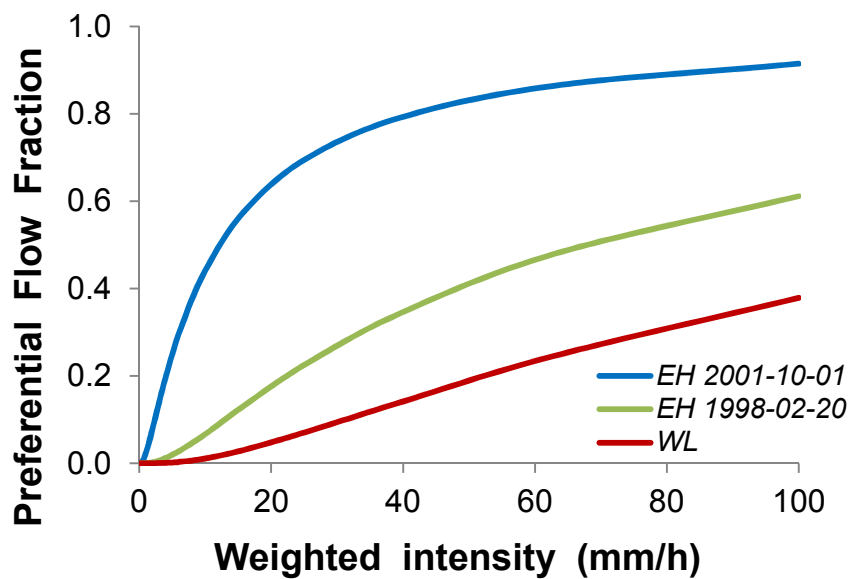


Figure 9. Model-predicted fraction of precipitation going to preferential flow based on data of Wilson and Luxmoore (1988), and optimizations for two storms in the data of Eguchi and Hasegawa (2008).